Article

Cell Reports

The Helicase PIF1 Facilitates Resection over Sequences Prone to Forming G4 Structures

Graphical Abstract

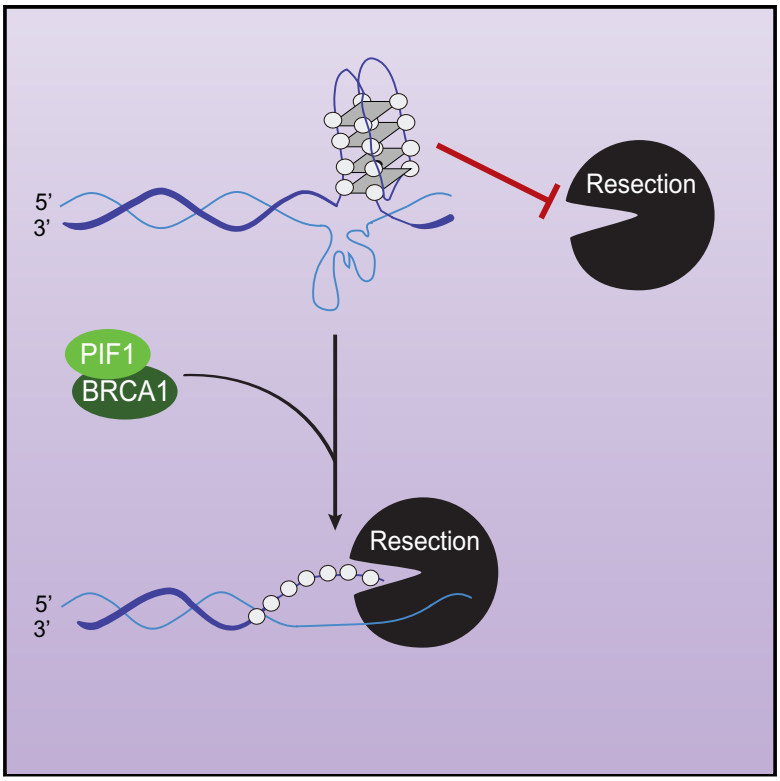

Authors

Sonia Jimeno, Rosa Camarillo, Fernando Mejías-Navarro, Maria Jesús Fernández-Ávila, Isabel Soria-Bretones, Rosario Prados-Carvajal, Pablo Huertas

Correspondence

sonia.jimeno@cabimer.es (S.J.), pablo.huertas@cabimer.es (P.H.)

In Brief

DNA resection machinery is well established in eukaryotes. However, little is known of the accessory factors required to resect over atypical DNA structures. In this paper, Jimeno et al. show that the helicase PIF1 facilitates resection, particularly at complex sequences that tend to form G-quadruplexes.

Highlights

- PIF1 is involved in DNA resection
- G-quadruplexes impair resection
- PIF1 is required to resect over sequences prone to forming G-quadruplexes
- PIF1 interacts with BRCA1 to resolve G-quadruplexes at DNA breaks

Jimeno et al., 2018, Cell Reports *24*, 3262–3273
September 18, 2018
https://doi.org/10.1016/j.celrep.2018.08.047

CellPress

OPEN ACCESS
CellPress

Cell Reports
Article

The Helicase PIF1 Facilitates Resection over Sequences Prone to Forming G4 Structures

Sonia Jimeno,[1,2,3,*] Rosa Camarillo,[1,2,3] Fernando Mejías-Navarro,[1,2] Maria Jesús Fernández-Ávila,[2] Isabel Soria-Bretones,[1,2,4] Rosario Prados-Carvajal,[1,2] and Pablo Huertas[1,2,5,*]

[1]Departamento de Genética, Universidad de Sevilla, Sevilla 41080, Spain
[2]Centro Andaluz de Biología Molecular y Medicina Regenerativa-CABIMER, Universidad de Sevilla-CSIC-Universidad Pablo de Olavide, Sevilla 41092, Spain
[3]These authors contributed equally
[4]Present address: The Campbell Family Institute for Breast Cancer Research, Princess Margaret Cancer Centre, University Health Network, Toronto, ON, Canada
[5]Lead Contact
*Correspondence: sonia.jimeno@cabimer.es (S.J.), pablo.huertas@cabimer.es (P.H.)
https://doi.org/10.1016/j.celrep.2018.08.047

SUMMARY

DNA breaks are complex lesions that can be repaired either by non-homologous end joining (NHEJ) or by homologous recombination (HR). The decision between these two routes of DNA repair is a key point of the DNA damage response (DDR) that is controlled by DNA resection. The core machinery catalyzing the resection process is well established. However, little is known about the additional requirements of DNA resection over DNA structures with high complexity. Here, we found evidence that the human helicase PIF1 has a role in DNA resection, specifically for defined DNA regions, such as those prone to form G-quadruplexes. Indeed, PIF1 is recruited to the site of DNA damage and physically interacts with proteins involved in DNA resection, and its depletion causes DNA damage sensitivity and a reduction of HR efficiency. Moreover, G4 stabilization by itself hampers DNA resection, a phenomenon suppressed by PIF1 overexpression.

INTRODUCTION

DNA is constantly exposed to different sources of DNA damage that can alter its chemical or physical structure. Within the different types of DNA lesions, DNA double-strand breaks (DSBs) are considered one of the most cytotoxic DNA injuries because they can lead to chromosomal aberrations and cell death. In order to maintain genomic stability, cells have developed a well-coordinated signaling cascade to sense and repair these DNA alterations known as the DNA damage response (DDR), which results in cell cycle arrest, senescence, activation of DNA repair pathways, stress responses, and/or apoptosis.

There are two main pathways to repair DSBs: non-homologous end joining (NHEJ) and homologous recombination (HR). On the one hand, NHEJ is based on the direct ligation of the broken DNA ends with little or no DNA end processing and it is the main mechanism to repair DSBs during G_0 and G_1 phases of the cell cycle (Davis and Chen, 2013). On the other hand, HR can accurately restore the DNA molecule using an intact homologous DNA sequence from the sister chromatid as the repair template (Jasin and Rothstein, 2013). Because HR prefers the sister chromatid to repair the DSB, this pathway is usually restricted to the S and G_2 phases of the cell cycle. If HR uses as donor sequence a DNA molecule different from the sister chromatid, loss of heterozygosity and even chromosome aberrations might be produced. Thus, the choice of the incorrect repair pathway might lead to genomic instability and, in consequence, to different diseases, including cancer. Additionally, DSBs might be sealed by a third type of repair pathways known as alternative-NHEJ (alt-NHEJ) or microhomology-mediated end joining (MMEJ). This alternative repair shares characteristics with both HR and NHEJ, uses short stretches of homology (microhomologies), and is always mutagenic (Sfeir and Symington, 2015).

DNA resection is the first step of HR and acts to promote this repair pathway and blocks NHEJ (Huertas, 2010; Symington, 2014). MMEJ also requires resection to expose the short homologies implicated in the repair process but to a much shorter extent (Sfeir and Symington, 2015). During resection, 5′ ends at DSBs are processed to obtain 3′ single-stranded DNA overhangs, which will invade a homologous DNA molecule and will act as primers for DNA synthesis. Resection is initiated by the MRE11-RAD50-NBS1 (MRN) complex that recognizes the DSB. Although MRE11 has endonuclease and exonuclease activities, it needs an additional factor, CtIP, to integrate several cellular signals in order to license resection only when the appropriate criteria are met (Cejka, 2015; Huertas, 2010; Makharashvili and Paull, 2015; Symington, 2014). This initial resection, termed short-range resection, is followed by an extension of the length of single-stranded DNA (ssDNA) in a process denominated long-range resection and catalyzed by either EXO1 or the helicase-nuclease pair BLM-DNA2 (Cejka, 2015; Huertas, 2010; Symington, 2014). This resection machinery is well conserved in all eukaryotes (Cejka, 2015; Huertas, 2010; Symington, 2014). Indeed, the human CtIP-MRN complex, or its counterpart Sae2-MRX in budding yeast, has been proven to constitute the minimal core resection initiation machinery *in vitro* (Anand et al., 2016; Nicolette et al., 2010; Shim et al., 2010).

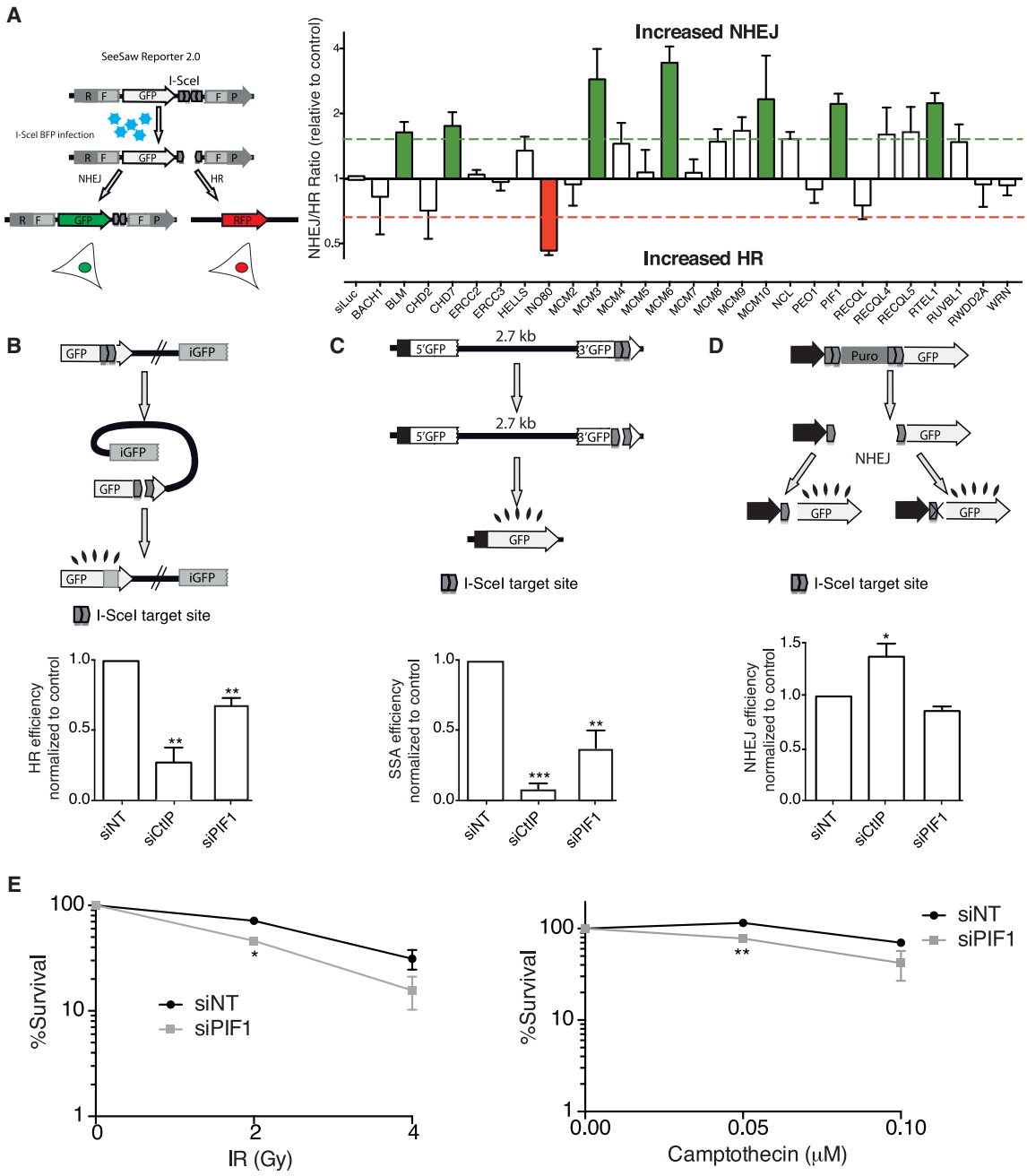

Figure 1. PIF1 Depletion Effect in Homologous Recombination and Survival to DNA Damage Induction

(A) An overview of the effect of the depletion of DNA helicases in DNA repair pathway choice. A schematic representation of the SeeSaw Reporter (SSR) is shown on the left. An I-SceI-induced DSB can be repaired by NHEJ, thus reconstructing an active GFP gene, or by homologous recombination using RFP fragments, thus creating a functional RFP gene. The results in the NHEJ/HR balance upon depletion of several DNA helicases, obtained from López-Saavedra et al. (2016), are shown on the right. Helicase genes for which depletion produces an unbalance toward increased HR are marked in red. Genes that encode pro-recombination helicases, i.e., NHEJ increased when they were downregulated, are marked in green. The plot represents the average and SD of three independent experiments

(B) Effect of PIF1 depletion in the DR-GFP reporter. A scheme of the reporter is shown on the top. Induction of a DSB using I-SceI meganuclease renders GFP-positive cells when the donor repeat (iGFP) is used in a gene conversion event. The efficiency of classical recombination was calculated as the percentage of GFP-positive cells in response to I-SceI expression upon downregulation of the indicated genes and normalized with the control. The average and SD of at least three independent experiments are shown.

(C) Same as (B) but using the single-strand annealing (SSA) reporter SA-GFP (top). In this case, the induction of a DSB located between two repeats in direct orientation will render GFP-positive cells only when intramolecular SSA takes place.

(legend continued on next page)

Although the central core of DNA resection is, therefore, well established, only little is known about how the velocity or processivity of DNA resection is modulated. As an illustration, the tumor suppressor BRCA1 affects the processivity of resection (Cruz-García et al., 2014). Such regulation will impact in the decision between HR and NHEJ but also between different HR subpathways (Ceccaldi et al., 2016). An important open question is whether the resection machinery needs additional effectors when faced with DNA regions of unusual configurations. One example would be G-quadruplexes (G4s), a DNA-secondary structure formed by four guanines associated through Hoogsteen hydrogen bonding that forms a G-quartet. The planar G-quartets stack on top of each other, giving rise to four-stranded helical structures (Lipps and Rhodes, 2009). Interestingly, recently it has been described that G-quadruplex-stabilizing compounds, such as pyridostatin (PYR) or CX-5461, are toxic to BRCA1-deficient cells (Xu et al., 2017; Zimmer et al., 2016). Thus, it remains possible that such toxicity might stem of an impairment of DNA resection in the presence of stable G4s and in the absence of processivity factors, such as BRCA1. Several helicases, including FANCJ, BLM, or WRN, have been shown to be able to unwind G4s (Mendoza et al., 2016; Murat and Balasubramanian, 2014; Sanders, 2010), but PIF1 helicase is considered the most specific and active on these structures (Bochman et al., 2012). The PIF1 family of helicases is highly conserved from yeast to humans and belongs to the superfamily of helicases 1 (Sabouri, 2017). PIF1 plays a role in multiple DNA transactions, including regulation of telomere homeostasis, replication induced by DSBs, transcription, and G4s resolution (Bochman et al., 2010; Gagou et al., 2014; Sabouri, 2017). This helicase binds to partially ssDNA and unwinds G4 structures suppressing G4-induced DNA damage (Sanders, 2010). Although the human genome encodes a single PIF1 gene, through alternative splicing, it produces two different transcripts. The long transcript produces PIF1α protein that is located in the nucleus, and the short one produces PIF1β that is found in the mitochondria (Sabouri, 2017).

Here, we report several lines of evidence that involve human PIF1α (from here on PIF1) in HR. Indeed, we propose an additional role for this helicase specifically at the resection step of the recombination process. Our data suggest that the helicase activity of PIF1 is particularly relevant for resection when G4 structures are stabilized on the DNA.

RESULTS AND DISCUSSION

PIF1 Is Involved in DNA DSB Repair

As previously mentioned, little is known of the additional factors that might help DNA resection machinery when confronted with DNA structures that are problematic. We reasoned that, as for almost every single DNA transaction, helicases would be in charge to reshape such unusual DNA configurations to facilitate the process. To find those helicases, we used an indirect approach and took advantage of the SeeSaw Reporter (SSR) (see Figure 1A, left) and the genome-wide screening we recently published (Gomez-Cabello et al., 2013; López-Saavedra et al., 2016) to look for different helicases in the choice between DSB repair pathways. This reporter analyses the choice between HR and NHEJ at very early stages; thus, it is particularly sensitive to changes in DNA resection velocity and/or processivity. Briefly, the SSR measures the balance between NHEJ and HR based on the accumulation of distinct fluorescent proteins (GFP for NHEJ events and red fluorescent protein (RFP) for HR events; in this case, a specific subpathway termed single-strand annealing [SSA]; Ceccaldi et al., 2016). Alterations of the normal balance toward a relative increase of HR or NHEJ can be detected using this reporter (Gomez-Cabello et al., 2013; Jimeno et al., 2015; López-Saavedra et al., 2016). As expected (see Figure 1A, right), depletion of either BLM or RTEL1, proteins with known roles in HR at the level of DNA resection, skewed the balance toward an increase in NHEJ (Gomez-Cabello et al., 2013; Gravel et al., 2008; Youds et al., 2010). Impairing the activity of the replication helicase minichromosome maintenance (MCM) by downregulation of almost any of its subunits also increased the relative contribution of NHEJ, probably due to an accumulation of S phase cells due to their role in DNA replication (Martinez et al., 2017). In addition, depletion of the chromatin remodeler INO80 showed the opposite effect, with an increased HR, suggesting a role of this helicase favoring NHEJ. This agrees with the fact that mutations in INO80-specific subunits in yeast impair the binding of Mre11, Ku80, and Mec1 kinase at the DSB, resulting in defective error-prone NHEJ (van Attikum et al., 2007; Chambers and Downs, 2012). Interestingly, the depletion of PIF1 had a similar phenotype of RTEL1 or BLM, suggesting a possible additional role of this DNA helicase in the HR branch of DSB repair (Figure 1A). In order to validate this idea, we first performed pathway-specific repair assays (Figures 1B–1D). In all cases, CtIP depletion, which blocks DNA resection, was used as a positive control. Briefly, in all reporters, a DSB is created by expression of the meganuclease I-SceI and its repair through one defined pathway renders the accumulation of GFP-positive cells. We observed that PIF1 depletion (for depletion efficiency, see Figures S1A–S1C) indeed impaired homology-directed repair, both the Rad51-independent single-strand annealing pathway, and also the Rad51-dependent gene conversion pathway (SA-GFP and DR-GFP reporters, respectively; Figures 1B and 1C). On the contrary, the impact on NHEJ was minimal (Figure 1D). Cell cycle is a major regulator of HR, as resection is limited or not existent in G1. However, we discarded that the observed HR defect was caused by an accumulation of G1 cells

(D) Same as (B), but using the NHEJ reporter EJ5-GFP. In this case, two I-SceI-induced DSBs could be repaired by conservative or mutagenic NHEJ granting the accumulation of functional GFP.
(E) Clonogenic assays of U2OS cells depleted with a siRNA against PIF1 or with control non-target siRNA (siNT) after treatment with different doses of IR (left) or camptothecin (CPT) (right).
(B–E) A Student's t test comparing cells depleted with a siRNA against PIF1 with control siNT was performed; statistical significance at *$p < 0.05$, **$p < 0.01$, or ***$p < 0.001$.
See also Figure S1.

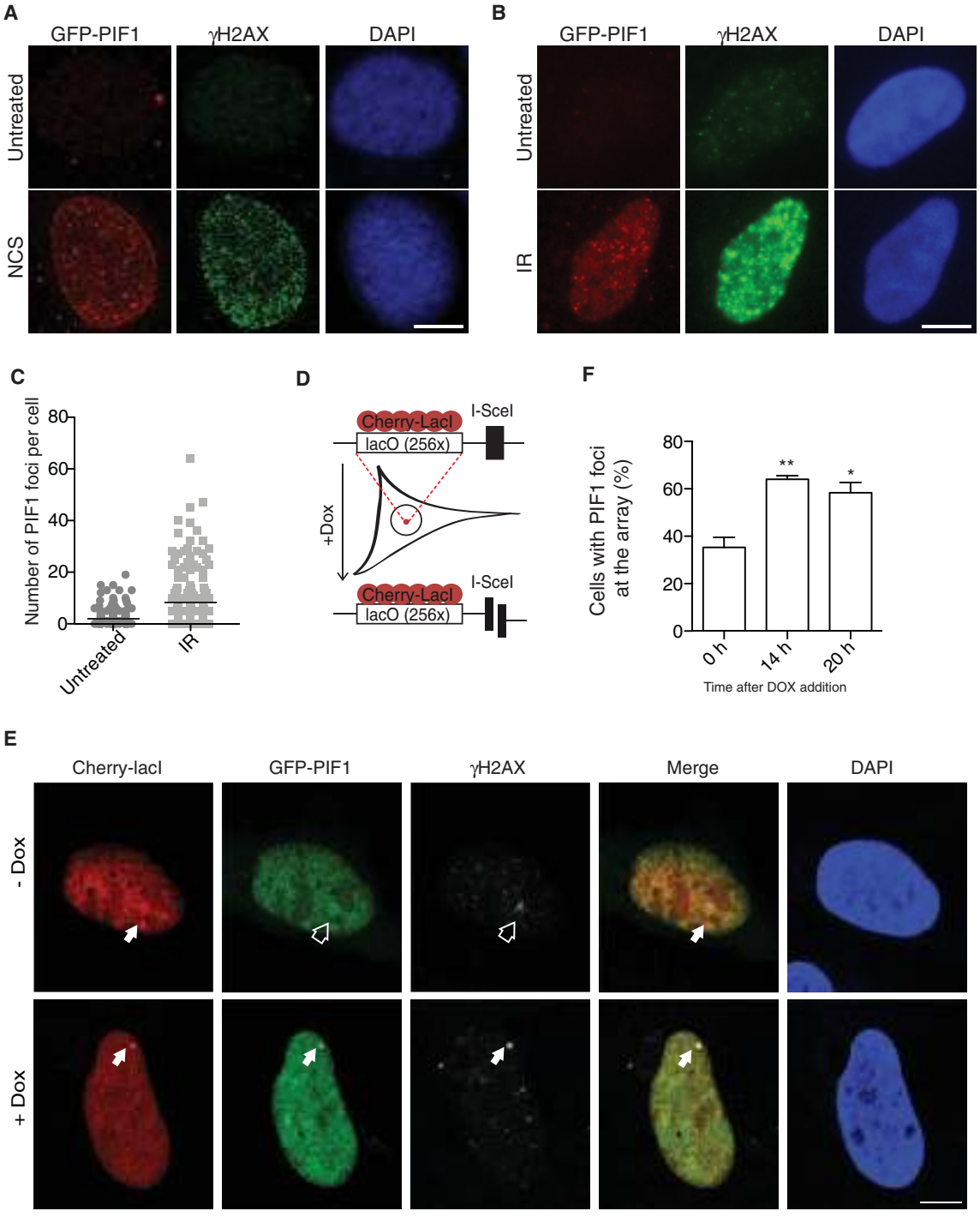

Figure 2. PIF1 Recruitment to DNA-Damage-Induced Foci

(A) GFP-PIF1 accumulation upon DNA damage induction with NCS using an antibody against GFP (shown in red). γH2AX accumulation was used as a control of DNA damage induction. Representative images of treated and untreated cells are shown. The scale bar represents 10 μm.

(B) Same as (A) but in cells exposed to 10 Gy of radiation. The scale bar represents 10 μm.

(C) Quantification of the number of GFP-PIF1 foci in untreated and irradiated, as indicated, in individual cells. The number of foci was scored automatically using Metamorph.

(D) Schematic representation of the experimental system to measure protein recruitment to DSBs. A single I-SceI target site is located close to 256 copies of the lacO sequence, allowing its visualization using a Cherry-LacI fusion. I-SceI is induced with the addition of doxycycline to induce a break.

(legend continued on next page)

(Figure S1D). Thus, we conclude that PIF1 affects the balance between HR and NHEJ mainly by facilitating DNA HR.

As expected from the repair defect, PIF1-depleted cells were mildly hyper-sensitive to agents that induce DSBs, such as ionizing radiation or camptothecin (Figure 1E). Our results are in agreement with the recently described new role of the PIF1 homolog Rrm3 in *Saccharomyces cerevisiae* in HR (Muñoz-Galván et al., 2017), suggesting that the role of PIF1 in HR might be conserved through evolution. Moreover, also in budding yeast, it has been shown that scPIF1, the other homolog of this helicase, is required for D-loop extension during break-induced replication (Saini et al., 2013; Wilson et al., 2013).

PIF1 Is Recruited to DNA-Damage-Induced Foci

Proteins involved in DSB repair are commonly recruited to broken chromatin and can be visualized under the microscope as foci. We tested whether this was also the case for PIF1. Upon the induction of DSBs with the DSB-inducing agent neocarzinostatin (NCS), we readily observed the focal accumulation of GFP-PIF1 using an anti-GFP antibody (Figure 2A; Figure S2A shows a GFP control). The same effect was observed upon treatment with ionizing radiation (IR) (Figure 2B; Figure S2B shows a GFP control). Computer-based automatic scoring of the number of PIF1 foci per cell agreed with an increase of PIF1 accumulation upon DNA damage (Figure 2C). To confirm that such a punctuated pattern reflected the recruitment of PIF1 to the sites of DNA breaks, we used the U2OS19ptight13 cells, in which a single DSB is induced with I-SceI upon the addition of doxycycline at a chromosomal location carrying 256 repeats of the lacO that can be visualized as the accumulation of a cherry-lacI discrete dot (Figures 2D and 2E; Lemaître et al., 2014). As shown in Figure 2F, there was some background binding of PIF1 prior doxycycline addition, likely due to the DNA structure created by the 256 repeats of the lacO. But importantly, a clear induction of GFP-PIF1 recruitment was observed upon DSB induction with doxycycline. Indeed, this accumulation mirrored DSB appearance, measured as γH2AX accumulation (Figures 2E, 2F, and S2C).

DNA Resection Requires PIF1

One likely explanation of the role of PIF1 in facilitating recombination and its recruitment to broken chromatin is that this helicase might be involved in DNA end resection. To test this idea, we studied replication protein A (RPA) foci formation upon ionizing radiation in PIF1 depleted cells. RPA is an ssDNA binding complex that accumulates at sites of DNA breaks as a direct consequence of DNA resection (Cejka, 2015; Huertas, 2010; Symington, 2014). Thus, the percentage of RPA-foci-positive cells is the gold standard readout of resection in mammalian cells. As shown in Figure 3A, depletion of PIF1 with two different small interfering RNAs (siRNAs) rendered a defect in resection efficiency that resembles, albeit to a lesser extent, downregulation of the key resection factor CtIP. To validate this observation, we used an alternative approach by quantifying the exposure of bromodeoxyuridine (BrdU)-labeled ssDNA in native conditions by fluorescence-activated cell sorting (FACS) as a proxy for ssDNA (Gómez-Cabello et al., 2017). BrdU epitope is hidden in the double-stranded structure of the DNA, so it cannot be detected by an antibody against it unless it is presented in a single-stranded form, either by denaturing the DNA or in native conditions by its exposure during DNA end resection. As seen in Figure 3B, in control cells, an increase of BrdU exposure in non-denaturing conditions after IR was observed. This was dependent on DNA end resection, as was completely abolished upon depletion of CtIP. Strikingly, PIF1 downregulation severely impairs BrdU exposure, as the signal remained close to the untreated control cells. Again, this defect was milder than the observed upon CtIP depletion, in agreement with an accessory role of PIF1 in resection. Both RPA foci formation and BrdU exposure depend at the same time on the number of breaks resected per cell and the extension of DNA resection. In order to analyze in more detail whether only resection initiation was impaired or whether also resection processivity was compromised, we used the single molecule analysis of resection tracks (SMART) technique, a high-resolution approach that measures resected DNA in individual DNA fibers (Cruz-García et al., 2014; Huertas and Cruz-Garcia, 2018; Figure 3C). Interestingly, not only the number of breaks resected was reduced upon PIF1 depletion, but the average length of ssDNA formed during resection was severely reduced when measured. Indeed, our data suggested that the main role of PIF1 is resection processivity, as in this case the observed defect was similar to that caused by CtIP depletion. This will agree with the idea that PIF1 is not an integral part of the resection machinery but an accessory factor that acts during resection extension, unwinding atypical DNA structures but has a very limited effect in the decision on which breaks will be resected.

In order to determine whether PIF1 was acting exclusively in one specific branch of resection, mainly the long-range resection catalyzed by either EXO1 or DNA2/BLM, we dissected its genetic relationship by targeting those factors with siRNA simultaneously to PIF1 depletion. We included also an siRNA against MRE11 as a key factor in the short-range resection machinery. We reasoned that, if PIF1 was exclusively in one of those pathways, its depletion would exacerbate the resection defect caused by downregulation of the other branch. As seen in the Figure 3D, PIF1 was epistatic with both EXO1 and DNA2, indicating it is likely acting on both pathways at the same time and that PIF1 depletion already hampers all long-range resection. Strikingly, PIF1 depletion mildly increased the defect observed upon MRE11 downregulation, likely due to targeting at the same time as both the short and long-range resection. Again,

(E) Immuno-fluorescence *in situ* hybridization (FISH) representative confocal images of Cherry-lacI in red, γH2AX (white), or GFP-PIF1 in green in cells expressing (+Dox) or not (−Dox) the I-SceI enzyme. An arrow points to the localization of the array in each image. Empty arrows mark where the array is, according to the LacI signal, on those cases in which no protein accumulation is observed (−DOX, without DSB induction). The scale bar represents 7.5 μm.
(F) Co-localization of the Cherry-LacI with GFP-PIF1. Cells were transfected with the plasmid containing GFP-PIF1 and treated with doxycycline for the indicated time. Values represent the average and SEM of three independent experiments.
One-way ANOVA analysis was performed to compare the indicated conditions in each graph. *$p < 0.5$; **$p < 0.01$. See also Figure S2.

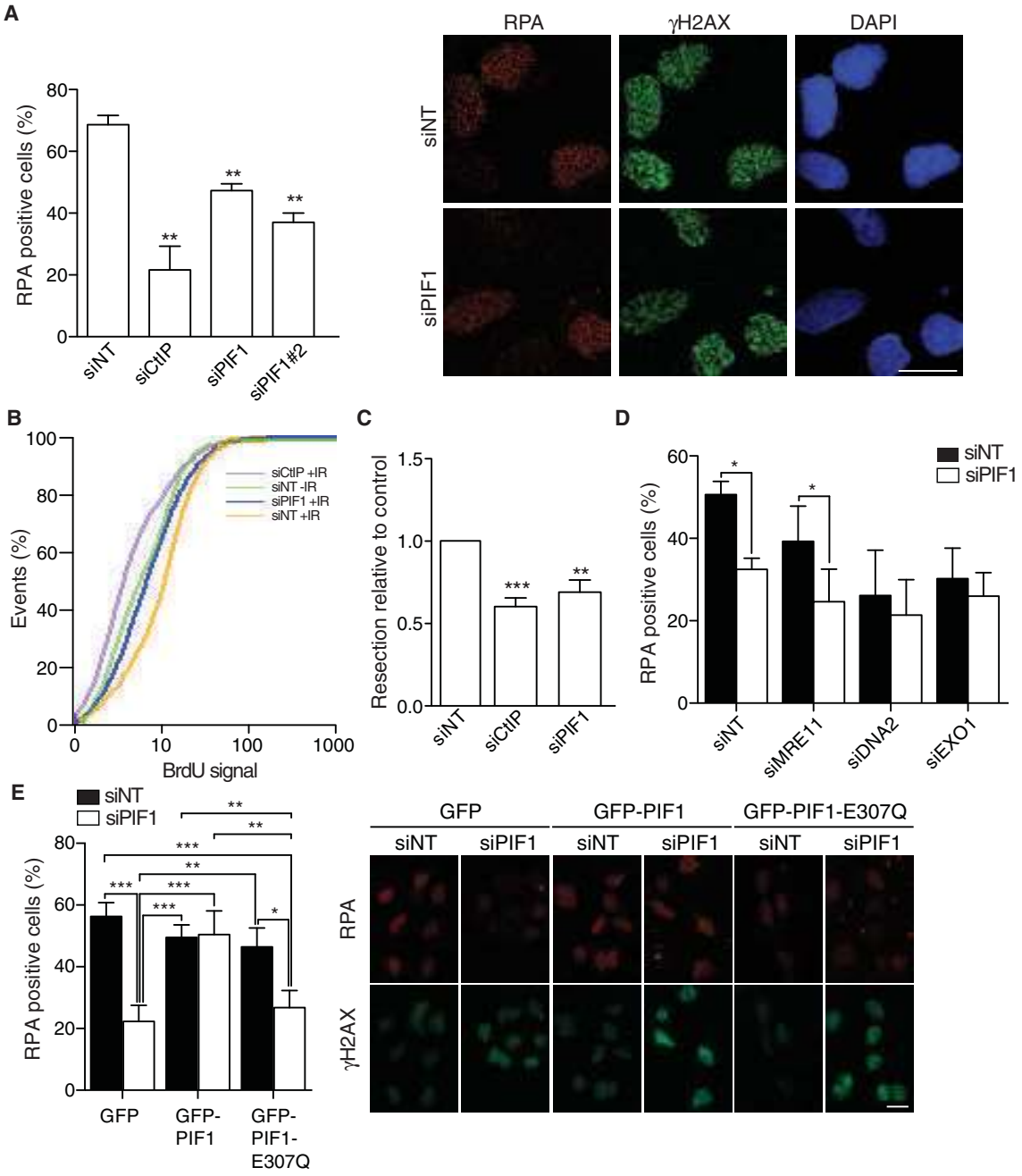

Figure 3. PIF1 Effect in DNA Resection

(A) DNA resection proficiency measured as the percentage of RPA-foci-positive cells in cells transfected with either an siRNA against PIF1, CtIP, or control siNT. The average and SD of three independent experiments are shown. Significance was determined by Student's t test comparing each condition to siNT cells. Representative images of the experiments are shown on the right side. The scale bar represents 25 μm.

(B) BrdU exposure under native conditions by FACS in cells transfected with the indicated siRNAs, either irradiated (+IR) or non-treated (−IR) as indicated. BrdU signal (x axis) is only observed in native conditions when resection exposes the BrdU epitope. Kolmogorov-Smirnov test was used to calculate the statistical significance of the different curves, with the following results: siNT-IR versus siNT+IR $p < 0.001$; siNT+IR versus siCtIP+IR $p < 0.001$; and siNT+IR versus siPIF1+IR $p < 0.001$.

(C) Resection length measured with SMART assay using DNA fibers extracted from U2OS downregulated for endogenous CtIP or PIF1. A siNT was used as control. The average and SEM of the median length in three independent experiments are plotted in the right graph. Other details are as in (A).

(D) RPA foci formation 1 hr after irradiation in cells cotransfected with the indicated pairs of siRNAs.

(legend continued on next page)

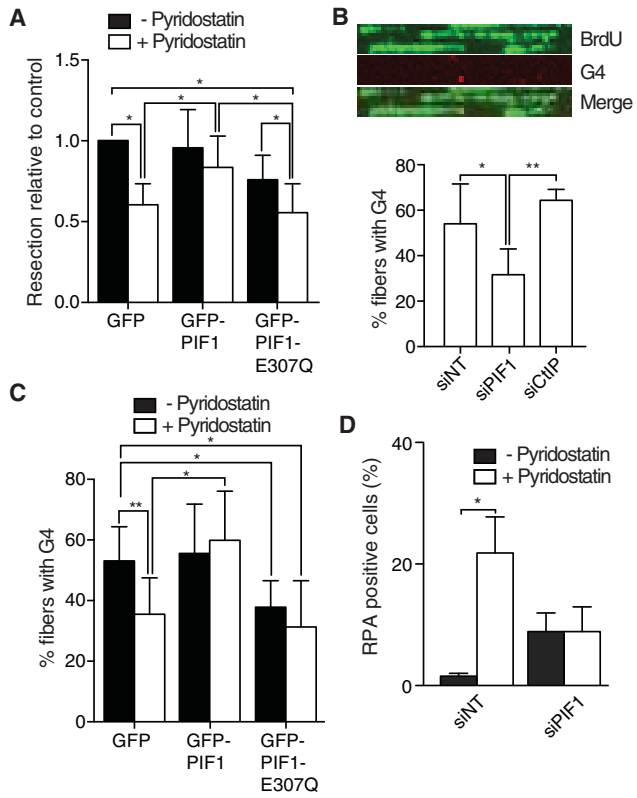

Figure 4. G4 Stabilization Impairs Resection

(A) SMART assay using DNA fibers extracted from irradiated U2OS overexpressing GFP-PIF or GFP as control and pretreated or not with pyridostatin. Other details are as in Figure 3C.

(B) G4 detection in individual ssDNA fibers. (Top) Representative ssDNA fiber containing G4 structures is shown. ssDNA was detected using the SMART assay in individual fibers with an anti-BrdU antibody (green) and G4 with a specific antibody (red). (Bottom) Quantification of the number of ssDNA fibers containing at least one G4 upon depletion with the indicated siRNAs is shown.

(C) Same as (B) but in cells treated or not with pyridostatin and bearing a GFP, a GFP-PIF1 wild-type, or helicase dead construct, as indicated.

(D) DNA resection, measured as the percentage of RPA-foci-positive cells, induced by pyridostatin treatment in cells transfected either with a siRNA against PIF1 or with control siNT. Other details are as in (A).

*$p < 0.05$; **$p < 0.01$.

these observations agree with an accessory role of PIF1 during resection extension. Therefore, we conclude that PIF1 is an accessory factor that is helping resection progression mainly at the level of long-range resection, both in the DNA2 and EXO1 branches. To be sure that the observed phenotype was due to PIF1 and not to an off-target effect, we study resection at the level of RPA foci formation in cells bearing siRNA-resistant, GFP-tagged versions of PIF1 gene. Indeed, the resection impairment caused by depletion of PIF1 was rescued by wild-type GFP-PIF1 (Figure 3E). More importantly, this was not observed with expression of a helicase dead version of the protein (Figures 3E and S3A). Thus, we can confirm that PIF1 is acting on long-range DNA end resection through its helicase activity, most likely by unwinding atypical DNA structures.

PIF1 Is Required to Resect over Sequences Prone to Forming G-Quadruplexes

We wondered then why this additional helicase might be needed for DNA end processing, i.e., which kind of atypical DNA species PIF1 is unwinding. Based on the role of PIF1 in facilitating DNA transactions on specific DNA structures, such as those DNA sequences prone to form G-quadruplexes, we reasoned that those structures might act as roadblocks for resection. Indeed, addition of the G4 stabilizer pyridostatin (Rodriguez et al., 2012), on its own, reduced the length of resected DNA formed upon induction of DSBs with ionizing radiation (Figure 4A). Interestingly, this decrease in the length of resected DNA was rescued when PIF1 was overexpressed (Figure 4A), but not by overexpression of a helicase-dead version of the protein. In order to validate this observation, we adjusted our SMART assay by adding a second primary antibody that recognizes G4s. Then, we could analyze in how many events resection went through one or more G4 structure(s) (Figure 4B). Strikingly, we quantified more than 50% of the resection events in which the processing happens over at least one sequence prone to form G4s. Moreover, this percentage dropped significantly if PIF1 was depleted. This drop was not simply due to the fact that the resection tracks are shorter, as CtIP depletion, which also reduced the length of resected DNA to a level comparable with PIF1 downregulation, does not cause this reduction in the % of G4-containing fibers (Figure 4B). Similarly, pyridostatin addition reduced the number of fibers containing G-quadruplex (Figure 4C), in agreement with the idea that the stabilization of such structure hampers the ability of the resection machinery to process DNA through them. Interestingly, wild-type PIF1 overexpression, but not a helicase-dead version of the protein, suppresses such reduction (Figure 4C). Thus, our data collectively suggested that sequences that tend to form G4s are indeed an impairment for DNA resection and PIF1 and, more importantly through its helicase activity, is involved in resolving these structures during DNA end processing. However, our data do not exclude the possibility that other factors might be also able to open G4s to facilitate resection.

Additionally, the simple addition of pyridostatin, with no additional source of DNA damage, caused an increase in spontaneous RPA foci formation that was completely dependent on PIF1 (Figure 4D). Interestingly, PIF1 depletion on its own increases the spontaneous levels of RPA in the absence of pyridostatin. We reasoned this reflects an increase in chances of specific DNA structure to break in the absence of PIF1. Thus, PIF1 depletion is acting at two levels. On one hand, its presence prevents spontaneous breakage of G4-forming sequences, but at the same time, PIF1 is required for their full processing. In the

(E) DNA resection proficiency measured as the percentage of RPA-foci-positive cells in cells expressing either GFP-PIF1 wild-type, a helicase dead version of the protein (E307Q), or GFP and transfected either with an siRNA against the 3′ UTR of PIF1 or a control siNT. Other details are as in (A). The scale bar represents 25 μm.

*$p < 0.05$; **$p < 0.01$; ***$p < 0.001$. See also Figure S3.

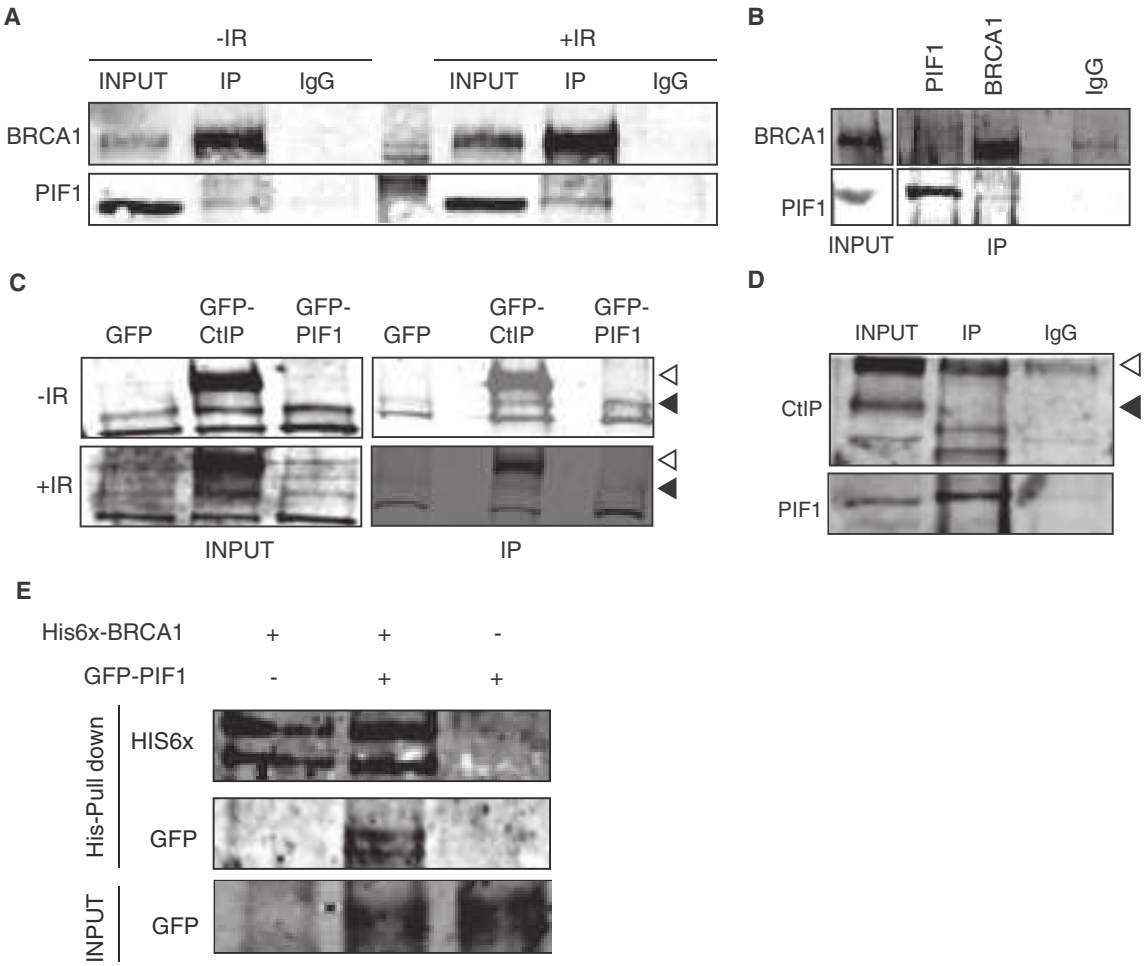

Figure 5. PIF1 Interaction with BRCA1 and CtIP Proteins

(A) Protein samples from U2OS cells were immunoprecipitated using an anti-BRCA1 antibody or a non-related immunoglobulin G (IgG) as a control in cells irradiated (right) or untreated (left). Inputs and immunoprecipitates were resolved in SDS-PAGE and blotted for BRCA1 and PIF1.

(B) Protein samples from U2OS cells bearing a GFP-PIF1 fusion were used for immunoprecipitation with antibodies against PIF1, BRCA1, or a control IgG, resolved in SDS-PAGE and blotted with the indicated antibodies.

(C) Cells bearing GFP-PIF1, GFP-CtIP, or GFP, as control, were used for immunoprecipitation using a GFP-trap both in untreated (−IR, top) or irradiated (+IR) conditions. Immunoprecipitated samples (IP) and protein inputs (INPUT) were resolved in SDS-PAGE and blotted with the indicated antibodies. Black triangle marks endogenous CtIP, whereas the empty triangle represents the GFP-CtIP fusion.

(D) Protein samples from U2OS cells harboring GFP-CtIP construct were used for immunoprecipitation with an antibody against PIF1 or a control IgG, resolved in SDS-PAGE, and blotted with the indicated antibodies. Other details are as in (C).

(E) Anti-His Dynabeads were incubated with His6×-BRCA1 or not as indicated. Afterward, *in vitro*-expressed GFP-PIF1 (+) or a mock control expressing a non-related protein (−) was added to the beads (see STAR Methods for details). After washing, proteins were released from the resin by boiling, resolved in SDS-PAGE, and blotted with the indicated antibodies. A western blot showing GFP-PIF1 input is shown at the bottom.

See also Figure S3.

absence of PIF1, more breaks will occur but would be subjected to limited resection, accounting for the mild increase in RPA foci. In the presence of pyridostatin in control cells, there will be many more breaks and those will be fully processed as PIF1 is present. The depletion of PIF1 is epistatic over pyridostatin treatment, as the G4s will be already causing breaks but cannot be completely processed in the absence of PIF1. This suggests that sequences prone to form G4s caused DNA lesions that are processed by the resection machinery in a PIF1-dependent fashion. Therefore, PIF1 prevents G4-mediated genomic instability by avoiding the appearance of breaks on those structures but also will affect how breaks at or close by to this G4-forming sequences will be repaired. Interestingly, this seems to be a conserved feature of PIF1 that has been shown to prevent G4-induced genomic rearrangements in yeast (Paeschke et al., 2013).

PIF1 Direct Interaction with the Resection Machinery Is Required for G4 Resolution

Our data suggested a functional relevance of PIF1 in DNA end resection, especially over regions with a tendency to form G4s.

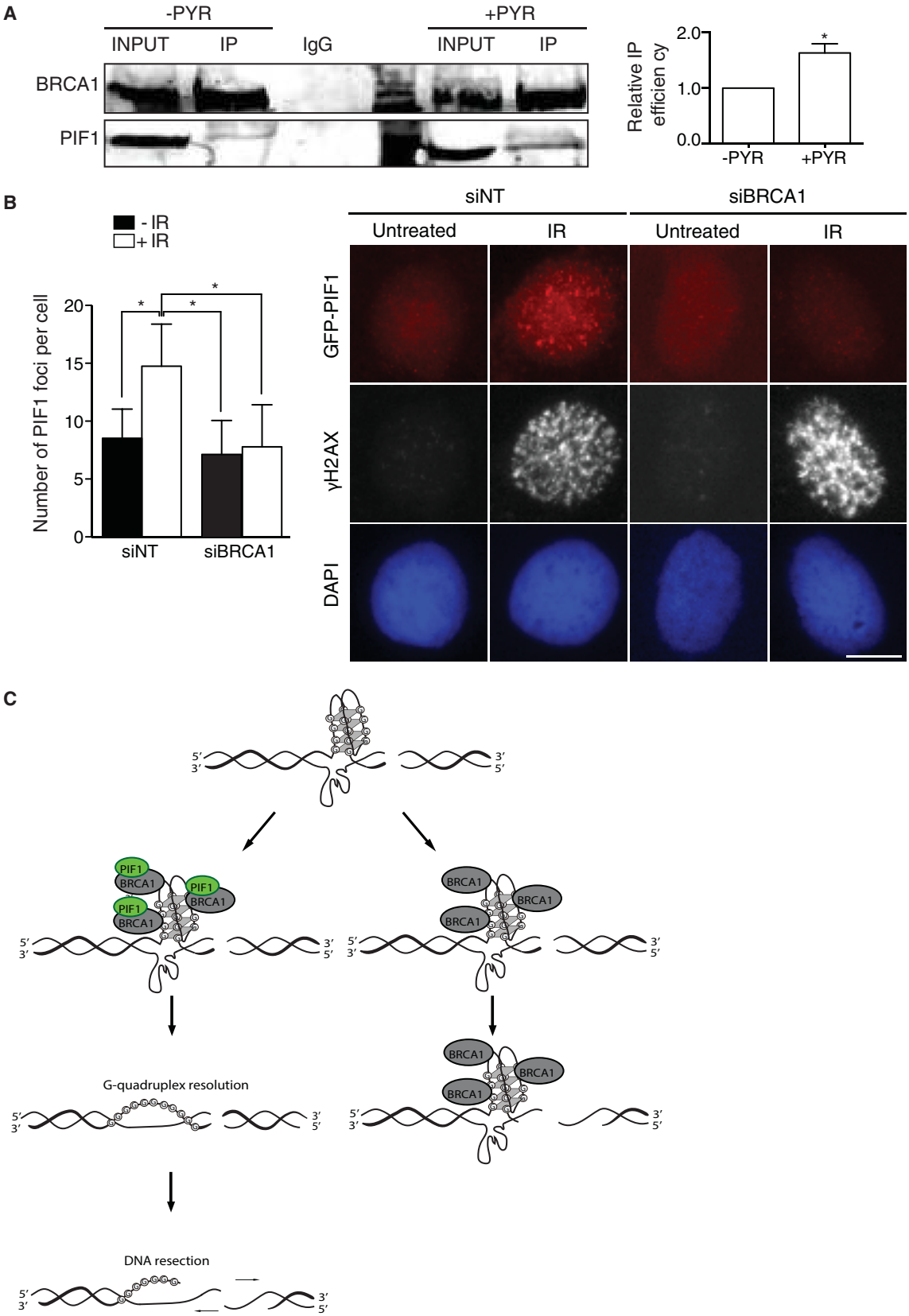

(legend on next page)

Interestingly, a recent study has shown that BRCA1 depletion causes sensitivity to pyridostatin (Xu et al., 2017; Zimmer et al., 2016). Considering the role of BRCA1 in facilitating resection, we speculated that these two factors might be connected in a more direct way. Thus, we first tested whether they physically interact. We could observe an interaction between BRCA1 and PIF1 both in untreated cells and in cells exposed to ionizing radiation (Figure 5A). Using antibodies against PIF1 or BRCA1, we could also confirm the interaction of those proteins by reciprocal co-immunoprecipitations (Figure 5B). Moreover, we could also observe the interaction between overexpressed GFP-PIF1 and the endogenous CtIP (Figure 5C). Reciprocally, using GFP-CtIP, we were able to immunoprecipitate endogenous PIF1 (Figure 5D). Interestingly, and different to BRCA1, we could never detect interaction between PIF1 and CtIP in cells that did not overexpress one of those factors. This might indicate that the interaction between PIF1 and CtIP is weaker than the one between BRCA1 and PIF1 or that it is indirect. To cement the idea that BRCA1 and PIF1 interact directly, we used recombinant histidine (HIS)-tagged BRCA1 and GFP-PIF1 and performed an *in vitro* binding assay. As shown in Figure 5E, purified HIS6×-BRCA1 efficiently pulled down recombinant GFP-PIF1. Considering the physical interaction between PIF1 and BRCA1, one possibility was that PIF1 depletion affected the steady-state levels of BRCA1 and that partial depletion of BRCA1 was the cause of the resection and recombination phenotypes. We excluded that possibility, as neither BRCA1 nor CtIP levels were affected by PIF1 depletion (Figure S3B).

Once the interaction of PIF1 with BRCA1 was established, we wanted to study whether this interaction was somehow related to the resolution of G4s. In order to test this hypothesis, we used total cell extracts from U2OS cells expressing GFP-PIF1 to co-immunoprecipitate BRCA1, both in the presence and absence of pyridostatin. Interestingly, there was a significant increase in the immunoprecipitation (IP) efficiency after treatment with pyridostatin compared to the mock control (Figure 6A), in agreement with a shared role in unwinding G4-forming sequences for BRCA1 and PIF1.

To confirm the relationship between PIF1 and BRCA1 in DNA resection, repair, and G4s resolution, we quantified PIF1 foci formation in U2OS cells expressing GFP-PIF1 either with or without irradiation in cells depleted or not of BRCA1. Interestingly, the relocalization of PIF1 after IR treatment, shown before in Figure 2, was dependent on BRCA1, because its depletion completely abolished such effect without affecting the basal levels of PIF1 foci (Figure 6B). Depletion of BRCA1 was verified by immunoblotting (see Figure S3B). From these results, we hypothesized that BRCA1 is needed to recruit PIF1 specifically to DNA damage sites. Interestingly, and in accordance with the functional relationship observed between PIF1 and BRCA1, a mutation in *PIF1* has been described to be present in patients that present a predisposition for breast cancer (Chisholm et al., 2012). This functional relationship of PIF1 and BRCA1 in resolving G4s specifically during HR might explain why BRCA1-deficient cells are sensitive to G4-stabilizing drugs (Xu et al., 2017; Zimmer et al., 2016). Moreover, it opens a window for therapeutic intervention in BRCA1-deficient tumors. Our data imply that G4-stabilizing agents will synergize with DSB-inducing treatments, such as radiotherapy, topoisomerase poisons, etc.

In summary, our data suggest a model (see Figure 6C) in which DNA resection is impaired by the presence of certain DNA structures, such as sequences with a tendency to form G4s. Thus, in order to resect over such structures, the helicase PIF1 is loaded to breaks located in the vicinity of such structures, a process that requires BRCA1. Once recruited, PIF1 would facilitate DNA resection through such special DNA structures. Despite a large overlap in G-quadruplexes unwinding by many helicases (Rhodes and Lipps, 2015), our data indicate a preponderant role of PIF1 during DSB processing. However, we cannot exclude that they also contribute to resection over this G4-forming region. This model explains why the absence of this helicase activity causes defective DNA end resection, HR impairment, and finally DNA damage sensitivity. The strong defect in DNA resection observed upon PIF1 depletion might suggest that this helicase is involved in the processing of breaks located close to other, still unknown, unusual DNA structures and not only in those that are close to sequences that tend to form G4. For example, it has been shown that PIF1 can unwind R-loops (Boulé and Zakian, 2007). Albeit we cannot discard the relevance of these additional structures, at least we can suggest its relevance for resection over sequences prone to form G4s. It has been proposed that there are more than 700,000 sequences with the ability to form such structures in the human genome (Chambers et al., 2015), so it is not surprising that over 50% of resected DNA tracts in our SMART assay contain at least one of them.

One interesting consideration is why G4 structures affect resection in the first place. G4s are supposed to form only when the DNA is already single stranded, as the interactions between both DNA strands will prevent its formation. Thus, it is likely that PIF1 role would be restricted to those physiological situations in which G4s appear, including during transcription, replication, and/or at telomeric DNA (Hänsel-Hertsch et al., 2017). Promoter regions are specially enriched in G4 structures, and over 40% of the genes have a G4 in its vicinity (Huppert

Figure 6. BRCA1 Loads PIF1 to Damaged Chromatin

(A) A BRCA1 antibody was used to immunoprecipitate BRCA1 and PIF1 after 4 hr of pyridostatin treatment or mock treatment. The average and SEM enrichment of three independent experiments are shown on the right. Significance was determined by Student's t test comparing the pyridostatin-treated conditions to mock-treated cells. *$p < 0.05$.

(B) Quantification of GFP-PIF1 foci formation after 10 Gy of irradiation (+IR) or in mock-treated cells (−IR) transfected either with a siRNA against BRCA1 or with control siNT. Representative images of the experiment are shown on the right. The scale bar represents 10 μm. GFP-PIF1 was detected using an anti-GFP antibody and is shown in red. γH2AX, in black and white, was used as a control of DSB induction. *$p < 0.05$

(C) Model describing the possible mechanism of PIF1 activity in DNA resection. PIF1 is recruited by BRCA1 to G4s in the vicinity of DSBs. Such recruitment promotes the unwinding of these structures and facilitates resection and homologous recombination. In the absence of PIF1, G4s remain, thus the resection machinery will have problems to function.

See also Figure S3.

and Balasubramanian, 2007). Indeed, G4s likely play regulatory roles during transcription (Kim, 2017). Recently, it has been shown that G4 indeed form *in vivo* at least at those promoter locations (Biffi et al., 2013; Hänsel-Hertsch et al., 2016). It is also worth mentioning that G4 can form in the ssDNA strand opposite to cotranscriptional R-loops helping to their stabilization (Kim, 2017). Indeed, and as mentioned above, PIF1 can remove also R-loops (Zhou et al., 2014). So either a G4-forming sequence, a G4-stabilized R-loop, or the combination of both can be the relevant structure that PIF1 must unwind for resection. Strikingly, it has been shown that transcribed regions are more likely to be resected and undergo HR than not transcribed regions (Aymard et al., 2014). So PIF1 importance might highlight the fact that it is especially required for resection under the context of transcribed chromatin, where G4 or other atypical structures, such as R-loops, are more likely to form. Additionally, it is clear that HR has an important role in rescuing and stabilizing stalled replication forks (Yeeles et al., 2013). In parallel, G4 structures are more evident in human cells during S phase, indicating they are forming during replication (Biffi et al., 2013). So again, PIF1 might be more important in this scenario of recombination-mediated rescue of stalled forks.

Based on the high degree of conservation between PIF1 orthologs (Bochman et al., 2010) and the involvement of the yeast counterpart in DSB repair (Saini et al., 2013; Wilson et al., 2013), it will be of interest analyzing whether the requirement of PIF1 to resect over G4 structures is conserved. Indeed, the role of RRM3 in sister chromatid exchange (Muñoz-Galván et al., 2017) might partially reflect a resection impairment. Less evidence is present of the hypothetical scPIF1 in resection, as it has been related with break-induced replication (BIR) (Saini et al., 2013; Wilson et al., 2013), which does not require extensive end processing. Moreover, the role of PIF1 in controlling the balance between repair pathways in regions containing G4s might explain why, in its absence, gross chromosomal rearrangements are increased when such structures are present (Paeschke et al., 2013).

STAR★METHODS

Detailed methods are provided in the online version of this paper and include the following:

- KEY RESOURCES TABLE
- CONTACT FOR REAGENT AND RESOURCE SHARING
- EXPERIMENTAL MODEL AND SUBJECT DETAILS
  - Cell lines and growth conditions
- METHOD DETAILS
  - siRNAs, plasmids and transfections
  - HR and NHEJ analysis
  - Clonogenic cell survival assays
  - RT-qPCR
  - SDS-PAGE and western blot analysis
  - Immunoprecipitation
  - Immunofluorescence and immuno-FISH
  - SMART
  - Flow Cytometry analysis
  - *In vitro* protein synthesis
  - Pull-down assay using recombinant proteins
- QUANTIFICATION AND STATISTICAL ANALYSIS

SUPPLEMENTAL INFORMATION

Supplemental Information includes three figures and one table and can be found with this article online at https://doi.org/10.1016/j.celrep.2018.08.047.

ACKNOWLEDGMENTS

We wish to thank Stephen P. Jackson and Evi Soutoglou for kindly providing GFP-PIF and U2OS19ptight13 cells, respectively. This work was funded by an R+D+I grant from the Spanish Ministry of Economy and Competitivity (SAF2016-74855-P). F.M.-N. and R.P.-C. are funded with FPU fellowships from the Spanish Ministry of Education, and I.S.-B. was funded with a fellowship from the University of Sevilla (V Plan Propio). CABIMER is supported by the regional government of Andalucia (Junta de Andalucía).

AUTHOR CONTRIBUTIONS

S.J. and R.C. performed all of the experiments showed, with the following exceptions. F.M.-N. helped with the PIF1 depletion SMART and analyzed HR and NHEJ upon PIF1 downregulation using reporters. M.J.F.-Á. contributed with the initial characterization of PIF1 role in resection by RPA. I.S.-B. helped R.C. with the analysis of the recruitment of GFP-PIF1 using the lacO array. R.P.-C. analyzed resection using FACS upon PIF1 depletion and helped with some RPA foci experiments. The project was conceived, designed, and supervised by P.H. with the help of S.J. R.C., S.J., and P.H., with some help from the other authors, contributed to the discussion of the results. P.H. wrote the paper, with the feedback of the rest of the authors.

DECLARATION OF INTERESTS

The authors declare no competing interests.

Received: April 3, 2018
Revised: July 16, 2018
Accepted: August 16, 2018
Published: September 18, 2018

REFERENCES

Anand, R., Ranjha, L., Cannavo, E., and Cejka, P. (2016). Phosphorylated CtIP functions as a co-factor of the MRE11-RAD50-NBS1 endonuclease in DNA end resection. Mol. Cell *64*, 940–950.

Aymard, F., Bugler, B., Schmidt, C.K., Guillou, E., Caron, P., Briois, S., Iacovoni, J.S., Daburon, V., Miller, K.M., Jackson, S.P., and Legube, G. (2014). Transcriptionally active chromatin recruits homologous recombination at DNA double-strand breaks. Nat. Struct. Mol. Biol. *21*, 366–374.

Bennardo, N., Cheng, A., Huang, N., and Stark, J.M. (2008). Alternative-NHEJ is a mechanistically distinct pathway of mammalian chromosome break repair. PLoS Genet. *4*, e1000110.

Biffi, G., Tannahill, D., McCafferty, J., and Balasubramanian, S. (2013). Quantitative visualization of DNA G-quadruplex structures in human cells. Nat. Chem. *5*, 182–186.

Bochman, M.L., Sabouri, N., and Zakian, V.A. (2010). Unwinding the functions of the Pif1 family helicases. DNA Repair (Amst.) *9*, 237–249.

Bochman, M.L., Paeschke, K., and Zakian, V.A. (2012). DNA secondary structures: stability and function of G-quadruplex structures. Nat. Rev. Genet. *13*, 770–780.

Boulé, J.B., and Zakian, V.A. (2007). The yeast Pif1p DNA helicase preferentially unwinds RNA DNA substrates. Nucleic Acids Res. *35*, 5809–5818.

Ceccaldi, R., Rondinelli, B., and D'Andrea, A.D. (2016). Repair pathway choices and consequences at the double-strand break. Trends Cell Biol. *26*, 52–64.

Cejka, P. (2015). DNA end resection: nucleases team up with the right partners to initiate homologous recombination. J. Biol. Chem. *290*, 22931–22938.

Chambers, A.L., and Downs, J.A. (2012). The RSC and INO80 Chromatin-Remodeling Complexes in DNA Double-Strand Break Repair (Elsevier).

Chambers, V.S., Marsico, G., Boutell, J.M., Di Antonio, M., Smith, G.P., and Balasubramanian, S. (2015). High-throughput sequencing of DNA G-quadruplex structures in the human genome. Nat. Biotechnol. *33*, 877–881.

Chisholm, K.M., Aubert, S.D., Freese, K.P., Zakian, V.A., King, M.C., and Welcsh, P.L. (2012). A genomewide screen for suppressors of Alu-mediated rearrangements reveals a role for PIF1. PLoS ONE *7*, e30748.

Cruz-García, A., López-Saavedra, A., and Huertas, P. (2014). BRCA1 accelerates CtIP-mediated DNA-end resection. Cell Rep. *9*, 451–459.

Davis, A.J.A., and Chen, D.J. (2013). DNA double strand break repair via non-homologous end-joining. Transl. Cancer Res. *2*, 130–143.

Gagou, M.E., Ganesh, A., Phear, G., Robinson, D., Petermann, E., Cox, A., and Meuth, M. (2014). Human PIF1 helicase supports DNA replication and cell growth under oncogenic-stress. Oncotarget *5*, 11381–11398.

Gomez-Cabello, D., Jimeno, S., Fernández-Ávila, M.J., and Huertas, P. (2013). New tools to study DNA double-strand break repair pathway choice. PLoS ONE *8*, e77206.

Gómez-Cabello, D., Checa-Rodríguez, C., Abad, M., Serrano, M., and Huertas, P. (2017). CtIP-specific roles during cell reprogramming have long-term consequences in the survival and fitness of induced pluripotent stem cells. Stem Cell Reports *8*, 432–445.

Gravel, S., Chapman, J.R., Magill, C., and Jackson, S.P. (2008). DNA helicases Sgs1 and BLM promote DNA double-strand break resection. Genes Dev. *22*, 2767–2772.

Hänsel-Hertsch, R., Beraldi, D., Lensing, S.V., Marsico, G., Zyner, K., Parry, A., Di Antonio, M., Pike, J., Kimura, H., Narita, M., et al. (2016). G-quadruplex structures mark human regulatory chromatin. Nat. Genet. *48*, 1267–1272.

Hänsel-Hertsch, R., Di Antonio, M., and Balasubramanian, S. (2017). DNA G-quadruplexes in the human genome: detection, functions and therapeutic potential. Nat. Rev. Mol. Cell Biol. *18*, 279–284.

Huertas, P. (2010). DNA resection in eukaryotes: deciding how to fix the break. Nat. Struct. Mol. Biol. *17*, 11–16.

Huertas, P., and Cruz-Garcia, A. (2018). Single molecule analysis of resection tracks. Methods Mol. Biol. *1672*, 147–154.

Huppert, J.L., and Balasubramanian, S. (2007). G-quadruplexes in promoters throughout the human genome. Nucleic Acids Res. *35*, 406–413.

Jasin, M., and Rothstein, R. (2013). Repair of strand breaks by homologous recombination. Cold Spring Harb. Perspect. Biol. *5*, a012740.

Jimeno, S., Fernández-Ávila, M.J., Cruz-García, A., Cepeda-García, C., Gómez-Cabello, D., and Huertas, P. (2015). Neddylation inhibits CtIP-mediated resection and regulates DNA double strand break repair pathway choice. Nucleic Acids Res. *43*, 987–999.

Kim, N. (2017). The interplay between G-quadruplex and transcription. Curr. Med. Chem. *25*, 1–19.

Lemaître, C., Grabarz, A., Tsouroula, K., Andronov, L., Furst, A., Pankotai, T., Heyer, V., Rogier, M., Attwood, K.M., Kessler, P., et al. (2014). Nuclear position dictates DNA repair pathway choice. Genes Dev. *28*, 2450–2463.

Lipps, H.J., and Rhodes, D. (2009). G-quadruplex structures: in vivo evidence and function. Trends Cell Biol. *19*, 414–422.

López-Saavedra, A., Gómez-Cabello, D., Domínguez-Sánchez, M.S., Mejías-Navarro, F., Fernández-Ávila, M.J., Dinant, C., Martínez-Macías, M.I., Bartek, J., and Huertas, P. (2016). A genome-wide screening uncovers the role of CCAR2 as an antagonist of DNA end resection. Nat. Commun. *7*, 12364.

Makharashvili, N., and Paull, T.T. (2015). CtIP: A DNA damage response protein at the intersection of DNA metabolism. DNA Repair (Amst.) *32*, 75–81.

Yeeles, J.T., Poli, J., Marians, K.J., and Pasero, P. (2013). Rescuing stalled or damaged replication forks. Cold Spring Harb. Perspect. Biol. *5*, a012815.

Martinez, M.P., Wacker, A.L., Bruck, I., and Kaplan, D.L. (2017). Eukaryotic replicative helicase subunit interaction with DNA and its role in DNA replication. Genes (Basel) *8*, E117.

Mendoza, O., Bourdoncle, A., Boulé, J.B., Brosh, R.M., Jr., and Mergny, J.L. (2016). G-quadruplexes and helicases. Nucleic Acids Res. *44*, 1989–2006.

Muñoz-Galván, S., García-Rubio, M., Ortega, P., Ruiz, J.F., Jimeno, S., Pardo, B., Gómez-González, B., and Aguilera, A. (2017). A new role for Rrm3 in repair of replication-born DNA breakage by sister chromatid recombination. PLoS Genet. *13*, e1006781.

Murat, P., and Balasubramanian, S. (2014). Existence and consequences of G-quadruplex structures in DNA. Curr. Opin. Genet. Dev. *25*, 22–29.

Nicolette, M.L., Lee, K., Guo, Z., Rani, M., Chow, J.M., Lee, S.E., and Paull, T.T. (2010). Mre11-Rad50-Xrs2 and Sae2 promote 5′ strand resection of DNA double-strand breaks. Nat. Struct. Mol. Biol. *17*, 1478–1485.

Paeschke, K., Bochman, M.L., Garcia, P.D., Cejka, P., Friedman, K.L., Kowalczykowski, S.C., and Zakian, V.A. (2013). Pif1 family helicases suppress genome instability at G-quadruplex motifs. Nature *497*, 458–462.

Pierce, A.J., Johnson, R.D., Thompson, L.H., and Jasin, M. (1999). XRCC3 promotes homology-directed repair of DNA damage in mammalian cells. Genes Dev. *13*, 2633–2638.

Rhodes, D., and Lipps, H.J. (2015). G-quadruplexes and their regulatory roles in biology. Nucleic Acids Res. *43*, 8627–8637.

Rodriguez, R., Miller, K.M., Forment, J.V., Bradshaw, C.R., Nikan, M., Britton, S., Oelschlaegel, T., Xhemalce, B., Balasubramanian, S., and Jackson, S.P. (2012). Small-molecule-induced DNA damage identifies alternative DNA structures in human genes. Nat. Chem. Biol. *8*, 301–310.

Sabouri, N. (2017). The functions of the multi-tasking Pfh1^{Pif1} helicase. Curr. Genet. *63*, 621–626.

Saini, N., Ramakrishnan, S., Elango, R., Ayyar, S., Zhang, Y., Deem, A., Ira, G., Haber, J.E., Lobachev, K.S., and Malkova, A. (2013). Migrating bubble during break-induced replication drives conservative DNA synthesis. Nature *502*, 389–392.

Sanders, C.M. (2010). Human Pif1 helicase is a G-quadruplex DNA-binding protein with G-quadruplex DNA-unwinding activity. Biochem. J. *430*, 119–128.

Sfeir, A., and Symington, L.S. (2015). Microhomology-mediated end joining: a back-up survival mechanism or dedicated pathway? Trends Biochem. Sci. *40*, 701–714.

Shim, E.Y., Chung, W.H., Nicolette, M.L., Zhang, Y., Davis, M., Zhu, Z., Paull, T.T., Ira, G., and Lee, S.E. (2010). Saccharomyces cerevisiae Mre11/Rad50/Xrs2 and Ku proteins regulate association of Exo1 and Dna2 with DNA breaks. EMBO J. *29*, 3370–3380.

Symington, L.S. (2014). End resection at double-strand breaks: mechanism and regulation. Cold Spring Harb. Perspect. Biol. *6*, a016436.

van Attikum, H., Fritsch, O., and Gasser, S.M. (2007). Distinct roles for SWR1 and INO80 chromatin remodeling complexes at chromosomal double-strand breaks. EMBO J. *26*, 4113–4125.

Wilson, M.A., Kwon, Y., Xu, Y., Chung, W.H., Chi, P., Niu, H., Mayle, R., Chen, X., Malkova, A., Sung, P., and Ira, G. (2013). Pif1 helicase and Polδ promote recombination-coupled DNA synthesis via bubble migration. Nature *502*, 393–396.

Xu, H., Di Antonio, M., McKinney, S., Mathew, V., Ho, B., O'Neil, N.J., Santos, N.D., Silvester, J., Wei, V., Garcia, J., et al. (2017). CX-5461 is a DNA G-quadruplex stabilizer with selective lethality in BRCA1/2 deficient tumours. Nat. Commun. *8*, 14432.

Youds, J.L., Mets, D.G., McIlwraith, M.J., Martin, J.S., Ward, J.D., ONeil, N.J., Rose, A.M., West, S.C., Meyer, B.J., and Boulton, S.J. (2010). RTEL-1 enforces meiotic crossover interference and homeostasis. Science *327*, 1254–1258.

Zhou, R., Zhang, J., Bochman, M.L., Zakian, V.A., and Ha, T. (2014). Periodic DNA patrolling underlies diverse functions of Pif1 on R-loops and G-rich DNA. eLife *3*, e02190.

Zimmer, J., Tacconi, E.M.C., Folio, C., Badie, S., Porru, M., Klare, K., Tumiati, M., Markkanen, E., Halder, S., Ryan, A., et al. (2016). Targeting BRCA1 and BRCA2 deficiencies with G-quadruplex-interacting compounds. Mol. Cell *61*, 449–460.

STAR★METHODS

KEY RESOURCES TABLE

REAGENT or RESOURCE	SOURCE	IDENTIFIER
Antibodies		
BrdU	GE Healthcare	Cat# RPN 202; RRID:AB_2314032
GFP	Santa Cruz	Cat# sc-8334; RRID:AB_641123
BRCA1	Santa Cruz	Cat# sc-6954; RRID:AB_626761
CtIP	Santa Cruz	Gift from Richard Baer
γH2AX	Cell Signaling	Cat# 2577; RRID:AB_2118010
Hsp70	Santa Cruz	Cat# sc-24; RRID:AB_627760
PIF1	Santa Cruz	Cat# sc-48377; RRID:AB_2164654
RPA2	Abcam	Cat# ab2175; RRID:AB_302873
Anti-His	GE Healthcare	Cat# 27-4710-01; RRID:AB_771435
α-tubulin (mouse)	Sigma Aldrich	Cat# T9026; RRID:AB_477593
Alexa Fluor 594 goat anti-mouse	Invitrogen	Cat# A-11032; RRID:AB_2534091
Alexa Fluor 488 goat anti-rabbit	Invitrogen	Cat# A-11034; RRID:AB_2576217
IRDye 680RD goat anti-mouse IgG (H+L)	Li-Cor	Cat# 926-68070; RRID:AB_10956588
AIRDye 800RD goat anti-rabbit IgG (H+L	Li-Cor	Cat# 926-32211; RRID:AB_621843
Chemicals, Peptides, and Recombinant Proteins		
Camptothecin	Sigma	Cat#C9911
Doxycycline	Sigma	Cat#D9891
Pyridostatin	Gentaur	Cat#A3742
His6x-BRCA1	Abcam	Cat#ab82204
Critical Commercial Assays		
PURExpress *in vitro* protein synthesis kit	New England Biolabs	Cat#E6800S
QuickChange Lightning Site-Directed Mutagenesis Kit	Agilent Technologies	Cat#210518
Experimental Models: Cell Lines		
U2OS	ATCC	Cat#HTB-96; RRID: CVCL_0042
U2OS GFP	Gift from Stephen P. Jackson	N/A
U2OS GFP-PIF1	Gift from Stephen P. Jackson (Rodriguez et al., 2012)	N/A
U2OS19ptight13	Gift from Evi Soutoglou (Lemaître et al., 2014)	N/A
U2OS-SAGFP	Bennardo et al., 2008	N/A
U2OS-EJ5	Bennardo et al., 2008	N/A
U2OS-DR-GFP	Pierce et al., 1999	N/A
Oligonucleotides		
See Table S1	N/A	N/A
Recombinant DNA		
pEGFP-C1	Clontech	Cat#6084-1
GFP-PIF1	Gift from Stephen P. Jackson (Rodriguez et al., 2012)	N/A
GFP-PIF1 E307Q	This paper	N/A
Software and Algorithms		
ImageStudio software	Li-Cor	N/A
NIS ELEMENTS Nikon Software	Nikon	
Adobe Photoshop CS4	Adobe	N/A
PRISM software	Graphpad	N/A
ModFit LT 3.0	Verity Software House	N/A

CONTACT FOR REAGENT AND RESOURCE SHARING

Further information and requests for resources and reagents should be directed to and will be fulfilled by the Lead Contact, Pablo Huertas (pablo.huertas@cabimer.es).

EXPERIMENTAL MODEL AND SUBJECT DETAILS

Cell lines and growth conditions

U2OS cell lines (female, RRID: CVCL_0042) were authenticated and obtained from the ATCC, then grown in DMEM (Sigma-Aldrich) supplemented with 10% fetal bovine serum (Sigma-Aldrich), 2 mM L-glutamine (Sigma-Aldrich), 100 units ml–1 penicillin and 100 μg ml–1 streptomycin (Sigma-Aldrich) at 37°C in 5% CO_2. U2OS stably expressing GFP or GFP-hPIF1 plasmids (Rodriguez et al., 2012) were grown in standard U2OS medium supplemented with 0.5 mg ml–1 G418 (Sigma) at 37°C in 5% CO_2. U2OS19ptight13 cells (Lemaître et al., 2014) were grown in the absence of phenol red and supplemented with 0.8 mg ml–1 G418 at 37°C in 5% CO_2. U2OS19ptight13 populations were generated by transfection of the different plasmids and selection with 1 μg ml–1 puromycin. Doxycyline (Sigma-Aldrich) was added to U2OS19ptight13 medium at a final concentration of 1 ug/mL 14/20 h prior fixation to induce I-SceI cutting.

METHOD DETAILS

siRNAs, plasmids and transfections

siRNA duplexes were obtained from Sigma-Aldrich or Dharmacon (See Key Resources Table) and were transfected using RNAiMax Lipofectamine Reagent Mix (Life Technologies), according to the manufacturer's instructions. Briefly, cells were seeded and grown for 24 h. The day of transfection, medium was replaced by fresh DMEM without antibiotics and cells were incubated with a mix of siRNA and Lipofectamine diluted in Opti-MEM. Cells were then incubated at 37°C for 6 h before replacing the media with fresh DMEM. All siRNA-mediated knockdowns were validated 48 h after transfection by western blot or RT-PCR.

GFP-PIF1 was a gift from Stephen P. Jackson (The Gurdon Institute, Cambridge). The helicase-dead GFP-hPIF1 mutant (GFP-PIF1 E307Q) was previously published (Gagou et al., 2014). It was obtained replacing a glutamic acid by a glutamine in the wild-type plasmid using the QuickChange Lightning Site-Directed Mutagenesis Kit (Agilent Technologies) according to manufacturer's instructions. Briefly, mutagenesis was performed using designed primers containing the desired mutations. After the PCR, DNA was amplified and sent to CNIO Genome Unit (Madrid, Spain) for DNA sequencing. Plasmid transfection of U2OS cells was carried out using FuGENE 6 Transfection Reagent (Promega) according to the manufacturer's protocol.

HR and NHEJ analysis

U2OS cells bearing a single copy integration of the reporters DR-GFP (Gene conversion) (Pierce et al., 1999), SA-GFP (SSA) (Bennardo et al., 2008) or EJ5-GFP (NHEJ) (Bennardo et al., 2008) were used to analyze the different DSB repair pathways. In all cases, 40,000 cells were plated in 6-well plates in duplicate. One day after seeding, cells were transfected with the indicated siRNA and the medium was replaced with fresh one 24h later. The next day, each duplicate culture was infected with lentiviral particles containing I-SceI–BFP expression construct at MOI 10 using 8 μg/ml polybrene in 1.5 mL of DMEM. Then, cells were left to grow for an additional 24 h before changing the medium for fresh DMEM. One day later, cells were washed with PBS, trypsinised, neutralized with DMEM, centrifuged for 5 min at 700 g, fixed with 4% paraformaldehyde for 20 min and collected by centrifugation. Then, cell pellets were washed once with PBS before resuspension in 150 μl of PBS. Samples were analyzed with a BD FACSAria with the BD FACSDiva Software v5.0.3. Four different parameters were considered: side scatter (SSC), forward scatter (FSC), blue fluorescence (407 nm violet laser BP, Filter 450/40), green fluorescence (488 nm blue laser BP Filter 530/30). Finally, the number of green cells from at least 10,000 events positives for blue fluorescence (infected with the I-SceI–BFP construct) was scored. The average of both duplicates was calculated for each sample of every experiment. To facilitate the comparison between experiments, this ratio was normalized with siRNA control. At least four completely independent experiments were carried out for each condition and the average and standard deviation is represented.

Clonogenic cell survival assays

To study cell survival after DNA damage, clonogenic assays were carried out seeding cells in 6-well plates at two different concentrations in triplicates. DSBs were produced by IR or by acute treatment with topoisomerase inhibitor camptothecin (CPT; C9911, Sigma). For IR, 250 and 500 transfected cells were seeded per well and, for drug treatments, 500 and 1,000 cells per well. The following day, cells were exposed to DNA damaging agents: 2 Gy, 4 Gy or mock treated or incubated for 1h with 0.01, 0.05 or 0.1 μM CPT or vehicle (DMSO) as control. After two washes with PBS, fresh medium was added and cells were incubated at 37°C for 7-14 days to allow colony formation. Afterward, cells were stained and visualized in solution of 0.5% Crystal Violet (1.15940.0025, Merck) and 20% ethanol (1.00983.1000, Merck). Once the colonies were stained, this solution was removed and

plates were washed with water. The surviving percentage at each dose was calculated by dividing the average number of visible colonies in treated versus control (untreated or vehicle-treated) dishes. The experiment was repeated three times, and the average and standard deviation for each condition was calculated.

RT-qPCR

RNA was extracted from U2OS cells using RNeasy Mini Kit (QIAGEN), and cDNA was produced from RNA samples with QuantiTect Reverse Transcription Kit (QIAGEN), according to the manufacturer's instructions. qPCR was performed using iTaq Universal SYBR Green Supermix (Bio-Rad) and the primers are listed in the Key Resources Table. The comparative threshold cycle (Ct) method was used to determine relative transcript levels, using β-actin expression as internal control. Expression levels relative to β-actin were determined with the formula $2^{-\Delta\Delta Ct}$. At least three completely independent replicas were performed for each case.

SDS-PAGE and western blot analysis

Protein extracts were prepared in 2 × Laemmli buffer (4% SDS, 20% glycerol, 125 mM Tris-HCl, pH 6.8) and passed 10 times through a 0.5 mm needle–mounted syringe to reduce viscosity. Proteins were resolved by SDS-PAGE and transferred to low fluorescence PVDF membranes (Immobilon-FL, Millipore). Membranes were blocked with Odyssey Blocking Buffer (LI-COR) and blotted with the appropriate primary antibody and infra-red dyed secondary antibodies (LI-COR) (See Key Resources Table). Antibodies were prepared in blocking buffer supplemented with 0.1% Tween-20. Membranes were air-dried in the dark and scanned in an Odyssey Infrared Imaging System (LI-COR), and images were analyzed with ImageStudio software (LI-COR).

Immunoprecipitation

IP with endogenous antibodies

U2OS cells or U2OS cells containing GFP or GFP-CtIP were harvested in lysis buffer (50 mM Tris-HCl, pH 7.4, 100 mM NaCl, 1 mM EDTA, 0.2% Triton X-100, 1X protease inhibitors (Roche), 1X phosphatase inhibitor cocktail 1 (Sigma)) and incubated for 30 minutes on ice with Benzonase (100 U/ml). Protein extract (1 mg) was then precleared with washed magnetic protein A Dynabeads (Novex) under gentle agitation at 4°C for 1 h. Precleared samples were then incubated with 10 μL of anti-PIF1 or anti-BRCA1 antibody or with an equivalent amount of IgG (Mouse of Rabbit) as negative control for 30 min at 4°C. The remaining beads were added to the mixture of proteins and antibody and then incubated overnight at 4°C with gentle agitation. Beads were then washed three times with lysis buffer, and the precipitate was eluted in 50 μL of Laemmli buffer 2x. At least three independent IPs were performed.

IP with GFP-TRAP

U2OS cells expressing GFP, GFP-CtIP or GFP-PIF1 were harvested in lysis buffer (10 mM Tris-HCl pH 7.5, 150 mM NaCl, 0.5 mM EDTA, 0.5% NP-40, 1 × protease inhibitors [Roche] and 1 × phosphatase inhibitor cocktail 1 [Sigma]) and incubated for 30 minutes on ice with Benzonase. Protein extract (1 mg) was mixed with 35 μL of washed magnetic anti-GFP beads (GFP-Trap_M, Chromotek) and incubated 2h at 4°C with gentle rocking. For the incubation NP-40 concentration is reduced to 0,2%. Beads were then washed 3 times with wash buffer (10 mM Tris-HCl pH 7.5, 150 mM NaCl, 0,5 mM EDTA, 0,01% NP-40, 1 × protease inhibitors [Roche] and 1 × phosphatase inhibitor cocktail 1 [Sigma]), and the precipitate was eluted in SDS sample buffer by boiling the beads and loaded onto a gel. For the pyridostatin treatment, the drug was added 4 hour prior to the initiation of the experiment and time points were taken as indicated in each case. The experiment was repeated three times.

Immunofluorescence and immuno-FISH

For RPA foci visualization, U2OS cells knocked-down for different proteins were seeded on coverslips. At 1 h after irradiation (10 Gy), coverslips were washed once with PBS followed by treatment with pre-extraction buffer (25 mM Tris-HCl, pH 7.5, 50 mM NaCl, 1 mM EDTA, 3 mM $MgCl_2$, 300 mM sucrose and 0.2% Triton X-100) for 5 min on ice. Cells were fixed with 4% paraformaldehyde (w/v) in PBS for 20 min. Following two washes with PBS, cells were blocked for 1 h with 5% FBS in PBS, co-stained with the appropriate primary antibodies (See Key Resources Table) in blocking solution overnight at 4°C or for 2 h at room temperature, washed again with PBS and then co-immunostained with the appropriate secondary antibodies in blocking buffer. After washing with PBS and dried with ethanol 70% and 100% washes, coverslips were mounted into glass slides using Vectashield mounting medium with DAPI (Vector Laboratories). RPA foci immunofluorescences were analyzed using a Leica Fluorescence microscope with a HCX PL APO 63x/1.4 OIL objective.

For PIF1 foci visualization, U2OS cells expressing GFP or GFP-hPIF1 were seeded on coverslips. The procedure was similar to the described for RPA foci visualization but using anti-GFP antibody.

For immuno-FISH, U2OS19ptight13 cells were co-transfected with a Cherry-lacI and GFP-PIF1α plasmids and treated or not with doxycycline for 14h or 20 h, as indicated. Then, cells were fixed with 4% paraformaldehyde for 15 min, permeabilized in 0.5% Triton for 15 min, blocked in 3% BSA in PBS 0.1% Tween and incubated with primary and secondary antibodies (See Key Resources Table) prepared in blocking solution for 1 h each. Coverslips were mounted using Vectashield mounting medium (Vector Laboratories) containing DAPI. To visualize and acquire the images, a LEICA confocal microscope TCS SP5 was used with a HCX PL APO lambda blue 63X/ 1.4 OIL objective.

In all cases, at least 100 cells were analyzed per condition and the experiments were replicated independently at least three times.

SMART

SMART (single-molecule analysis of resection tracks) was performed as described (Huertas and Cruz-Garcia, 2018). Briefly, cells were grown in the presence of 10 μM BrdU for less than 24 h. Cultures were then irradiated (10 Gy) and harvested after 1 h. Cells were embedded in low-melting agarose (Bio-Rad), followed by DNA extraction. DNA fibers were stretched on silanized coverslips, baked for 2 hr at 60°C and incubated directly without denaturation with an anti-BrdU mouse monoclonal (See Key Resources Table). After washing with PBS, coverslips were incubated with the secondary antibody (See Key Resources Table). Finally, coverslips were mounted with ProLong Gold Antifade Reagent (Molecular Probes) and stored at −20°C. Samples were observed with a Nikon NI-E microscope and PLAN FLOUR40 × /0.75 PHL DLL objective and images were taken and processed with the NIS ELEMENTS Nikon Software. For each experiment, at least 200 DNA fibers were analyzed, and the length of the fibers was measured with Adobe Photoshop CS4. At least three independent replicas per condition were performed. For the pyridostatin treatment, the drug was added 1 hour prior to the irradiation.

Flow Cytometry analysis

Cell cycle analysis

Cells were fixed with cold 70% ethanol overnight, incubated with 250 μg ml^{-1} RNase A (Sigma) and 10 μg ml^{-1} propidium iodide (Fluka) at 37°C for 30 min and analyzed with a FACSCalibur (BD). Cell cycle distribution data were further analyzed using ModFit LT 3.0 software (Verity Software House Inc). The experiments were repeated three times.

Flow Cytometric Analysis of DNA End Resection

Cells were grown in the presence of 10 μM bromodeoxyuridine (BrdU; GE Healthcare) for 16–18 hr and then detached using accutase (eBioscence). Cells were fixed with 4% paraformaldehyde for 10 min at 4°C, permeabilized with 0.*1% Triton X-100* in *PBS, washed in PBS,* and then blocked with 5% FBS in PBS. After blocking, cells were incubated with an anti-BrdU mouse monoclonal for 1–2 hr at room temperature and then with the appropriate secondary antibody for 30 min at room temperature. Cells were then washed and resuspended in PBS. Samples were analyzed with a BD FACSCalibur Flow Cytometer (BD Biosciences, Ref: 342975). At least 10,000 events were recorded for each sample and the experiments were repeated independently three times.

In vitro protein synthesis

GFP-hPIF1 was synthesized *in vitro* using the PURExpress *in vitro* protein synthesis kit (E6800S, New England BioLabs). A PCR-amplified DNA from GFP-hPIF1 plasmids (Rodriguez et al., 2012) using appropriate primers to insert a T7 promoter and an *Escherichia coli* ribosome entry site upstream of the gene-specific sequence was used as a template, according to the manufacturer's instructions. Protein synthesis was carried out using 250 ng of DNA template in a final volume of 25 μl. Reactions without DNA were set up as negative controls.

Pull-down assay using recombinant proteins

To study PIF1 direct interaction with BRCA1, 250 ng of purified His6x-BRCA1 (ab82204, Abcam) resuspended in 200 μl of binding buffer (50 mM Sodium Phosphate pH 8.0, 300 mM NaCl, 0.01% Tween-20) was incubated with 50 μl of pre-equilibrated magnetic Dynabeads His-Tag Isolation & Pulldown (Life Technologies, 10103D) in a rocking wheel for 1h at 4°C. After incubation, *in vitro* synthesized GFP-hPIF1 resuspended in 200 μL of pull-down buffer (3.25 mM Sodium Phosphate pH 7.4, 70 mM NaCl, 0.01% Tween-20) was incubated at 4°C for 1h with the His6-BRCA1 bound to the Dynabeads. A mock sample of the *in vitro* protein synthesis using a non-related template was incubated with His6x-BRCA1-dynabeads as a control. Additionally, a third sample with GFP-PIF1 incubated with Dynabeads without the His6x-BRCA1 was prepared. The mixture was washed three times with binding buffer, resuspended in elution buffer (2x SDS-PAGE sample loading buffer and binding buffer supplemented with 300 mM Imidazole) and boiled for 2 min at 100°C to obtain the proteins. Finally, precipitated proteins were resolved by SDS-PAGE and analyzed by western blotting as described.

QUANTIFICATION AND STATISTICAL ANALYSIS

Statistical significance was determined with a Student's t test using PRISM software (Graphpad Software Inc.). Statistically significant differences were labeled with one, two or three asterisks if $p < 0.05$, $p < 0.01$ or $p < 0.001$, respectively. Specific replicate numbers (N) for each experiment can be found in the corresponding figure legends. In all figures, means are plotted and standard deviation (SD) is represented as error bars.